NeuroImage: Clinical 37 (2023) 103285

Contents lists available at ScienceDirect

NeuroImage: Clinical

journal homepage: www.elsevier.com/locate/ynicl

Event-based modeling of T1-weighted MRI is related to pathology in frontotemporal lobar degeneration due to tau and TDP

Christopher A. Olm [a,b], Sarah E. Burke [b], Claire Peterson [b,c,1], Edward B. Lee [d], John Q. Trojanowski [d,2], Lauren Massimo [b], David J. Irwin [b,c], Murray Grossman [b], James C. Gee [a,*]

[a] Penn Image Computing and Science Laboratory, Department of Radiology, University of Pennsylvania, Philadelphia, PA, United States
[b] Penn Frontotemporal Degeneration Center, Department of Neurology, University of Pennsylvania, Philadelphia, PA, United States
[c] Digital Neuropathology Laboratory, Department of Neurology, University of Pennsylvania, Philadelphia, PA, United States
[d] Department of Pathology and Laboratory Medicine, University of Pennsylvania, Philadelphia, PA, United States

ARTICLE INFO

Keywords:
Event based model
Frontotemporal lobar degeneration
Structural MRI
Dementia
Biomarkers

ABSTRACT

Background: In previous studies of patients with frontotemporal lobar degeneration due to tau (FTLD-tau) and FTLD due to TDP (FTLD-TDP), cortical volumes derived from T1-weighted MRI have been used to identify a sequence of volume loss according to arbitrary volumetric criteria. Event-based modeling (EBM) is a probabilistic, generative machine learning model that determines the characteristic sequence of changes, or "events", occurring during disease progression. EBM also estimates an individual patient's disease "stage" by identifying which events have already occurred. In the present study, we use an EBM analysis to derive stages of regional anatomic atrophy in FTLD-tau and FTLD-TDP, and validated these stages against pathologic burden.

Methods: Sporadic autopsy-confirmed patients with FTLD-tau (N = 42) and FTLD-TDP (N = 21), and 167 healthy controls with available T1-weighted images were identified. A subset of patients had quantitative digital histopathology of cortex performed at autopsy (FTLD-tau = 30, FTLD-TDP = 17). MRI images were processed, producing regional measures of cortical volumes. K-means clustering was used to find cortical regions with similar amounts of GM volume changes (n = 5 clusters). EBM was used to determine the characteristic sequence of cortical atrophy of identified clusters in autopsy-confirmed FTLD-tau and FTLD-TDP, and estimate each patient's disease stage by cortical volume biomarkers. Linear regressions related pathologic burden to EBM-estimated disease stages.

Results: EBM for cortical volume biomarkers generated statistically robust characteristic sequences of cortical atrophy in each group of patients. Cortical volume-based EBM-estimated disease stage was associated with pathologic burden in FTLD-tau ($R2 = 0.16$, $p = 0.017$) and FTLD-TDP ($R2 = 0.51$, $p = 0.0008$).

Conclusions: We provide evidence that EBM can identify sequences of pathologically-confirmed cortical atrophy in sporadic FTLD-tau and FTLD-TDP.

Abbreviations: EBM, event-based modeling; FTLD-tau, frontotemporal lobar degeneration due to tau; FTLD-TDP, frontotemporal lobar degeneration due to TDP; GM, gray matter; MMSE, mini mental state exam; bvFTD, behavioral variant frontotemporal degeneration; PPA, primary progressive aphasia; PiD, Pick's disease; PSP, progressive supranuclear palsy; CBD, corticobasal degeneration; ROI, region of interest; MCMC, Markov Chain Monte Carlo; %AO, percent area occupied; QC, quality control; AD, Alzheimer's disease; PCA, principal component analysis; WCSS, within cluster sum of squares; AIC, Akaike information criterion; aCING, anterior cingulate; MFC, middle frontal cortex; OFC, orbitofrontal cortex; SMTC, superior-middle temporal cortex; ANG, angular gyrus.

* Corresponding author at: Richards Medical Research Laboratories, 3700 Hamilton Walk, 6th Floor, Philadelphia, PA 19104, United States.
E-mail addresses: olm@pennmedicine.upenn.edu (C.A. Olm), Sarah.Burke@pennmedicine.upenn.edu (S.E. Burke), cspeters@uab.edu (C. Peterson), Edward.Lee@pennmedicine.upenn.edu (E.B. Lee), Lauren.Massimo@pennmedicine.upenn.edu (L. Massimo), dirwin@pennmedicine.upenn.edu (D.J. Irwin), mgrossma@pennmedicine.upenn.edu (M. Grossman), gee@upenn.edu (J.C. Gee).
[1] Present address: The University of Alabama at Birmingham, Birmingham, AL, USA.
[2] Posthumous.

https://doi.org/10.1016/j.nicl.2022.103285
Received 22 July 2022; Received in revised form 5 December 2022; Accepted 6 December 2022
Available online 7 December 2022

1. Introduction

Neurodegenerative diseases are progressive in nature. Objective methods for characterizing progression during life are challenging yet vital to interpreting data from disease-modifying clinical treatment trials (Staffaroni et al., 2019). Machine learning methods are increasingly being used to tackle such problems in precision medicine; providing estimates of disease severity and prognosis while reducing sources of bias (Rajkomar et al., 2019). One such method, event-based modeling (EBM), is a probabilistic generative model that determines the characteristic sequence of changes, dubbed "events," that occur during the disease course (Fonteijn et al., 2011, 2012; Venkatraghavan et al., 2019; Young et al., 2014, Young et al., 2018). EBM models changes in biomarkers as discrete occurrences in a sequence during the course of progressive disease (Fonteijn et al., 2012). EBM requires only a binary assessment of either "control" or "not", minimizing the need for subjective clinical evaluations. By iteratively switching the order of potential biomarker changes, EBM uncovers the most likely, "characteristic", sequence of events. Furthermore, EBM estimates the current best fit "stage" for each patient; providing an estimate for the patient's current disease severity, and by extension, the next likely changes to occur during disease.

Frontotemporal lobar degeneration (FTLD) is an ideal model for evaluating modern staging methods because, unlike Alzheimer's disease (AD), it is often a monoproteinopathy. Therefore, in protein-targeted treatment trials, it is likely that only one type of pathologic inclusion is responsible for disease progression, making interpretation of changes over the course of disease more straightforward. In this study, we evaluate FTLD associated with misfolded tau protein (FTLD-tau) (Mackenzie et al., 2009, 2010) and with misfolded tar-DNA binding protein (FTLD-TDP) (Mackenzie et al., 2009; Neumann et al., 2006). In both diseases, pathologic burden remains the "gold standard" for disease severity, though identifying *in vivo* markers of disease severity is important for potential clinical treatment trials. T1-weighted MRI is widely available, non-invasive, repeatable, and can be used to monitor disease by capturing antemortem changes in gray matter (GM) structure by estimating regional volumes and cortical thickness. Such measures have been associated with pathologic burden in FTLD-tau and FTLD-TDP in behavioral variant frontotemporal degeneration (bvFTD) (Brettschneider et al., 2014; Irwin et al., 2016a; Irwin et al., 2018; Whitwell et al., 2011), primary progressive aphasia (PPA) (Giannini et al., 2019a), and in groups of participants with FTLD-tau and FTLD-TDP pathology regardless of specific clinical presentation (Burke et al., 2022; Whitwell et al., 2009a).

A common application of machine learning methods is to identify shared features in a large set of data points to reduce these into a smaller set of factors of interest. K-means clustering is a widely used machine learning clustering method that has the flexibility to form a tractable number of clustered regions from smaller regions that may be anatomically distributed. A comparable approach uses principal component analysis (PCA) to identify clusters of imaging features that can sort patients into groups (López et al., 2011; Wilson et al., 2009). Regardless of the specific approach, clustering is important for generating a reasonable number of region sets for data-driven sequencing models like EBM when patient data are limited, such as when examining patient groups with rare conditions with a difficult to acquire gold standard. To sequence cortical GM changes, studies using EBM and other similar methods often use pre-existing coarsely defined atlases or lobe-wise summaries to generate cortical GM biomarkers (Fonteijn et al., 2012; Panman et al., 2021; Young et al., 2014). However, results using such methods tend to generate characteristic sequences with high positional variance which leads to some difficulty in interpretation of the resulting sequence. Furthermore, whole-lobe measurements may not respect disease boundaries to adequately capture variance across the patient sample.

In this study, we used machine learning to identify sets of cortical regions based on amount of GM atrophy and then sequence these clusters using EBM. We hypothesized that, in groups of autopsy-confirmed FTLD-tau and FTLD-TDP participants, k-means clustering would identify sets of cortical regions in T1-weighted MRIs that EBM would then use to generate characteristic sequences of cortical volume loss. EBM also generates a disease severity estimate for each patient by determining which change events have already occurred in each patient and which have yet to occur. As later estimated stages should indicate more advanced disease, we hypothesized that patients with later estimated stages will have greater pathologic burden found at autopsy, and perhaps lower scores on tests of general cognitive functioning such as mini mental state exam (MMSE).

2. Materials and methods

2.1. Participants

We used the Penn Integrated Neurodegenerative Disease Database (INDD) (Toledo et al., 2014) to identify 42 patients with FTLD-tau pathology (Pick's Disease (PiD) N = 10, progressive supranuclear palsy (PSP) N = 20, corticobasal degeneration (CBD) N = 12), 21 patients with FTLD-TDP pathology (Type A, N = 6; Type B, N = 5; Type C, N = 6; Type E, N = 4) and 170 age- and education-matched healthy controls with at least one antemortem high resolution T1-weighted image (see Table 1 for a summary of demographic information). Expert pathologists confirmed pathological diagnosis (EBL, JQT) according to published criteria (Toledo et al., 2014). Experienced cognitive neurologists (MG, DJI, LM) at the Penn Cognitive Neurology Outpatient Clinic diagnosed patients clinically with published criteria for phenotypes confirmed at a multidisciplinary consensus meeting. Exclusion criteria included more than minimal co-pathology burden, or having any clinical or pathological evidence of stroke, significant head injury, infection, immune-mediated disorder, or intracranial mass or hydrocephalus. We also excluded participants with a genetic mutation associated with FTLD (Wood et al., 2013), to avoid potential confounding factors as participants with genetic mutations have been shown to have unique clinical, pathological, and imaging characteristics relative to those with sporadic FTLD (Capozzo et al., 2017; Janssen et al., 2002; Whitwell et al., 2012). Patients clinically diagnosed with amyotrophic lateral sclerosis (ALS) without a clinically noted cognitive or social deficit and/or without a low score of the Edinburgh Cognitive and Behavioral ALS Screen (ECAS) during life were excluded. All participants underwent an informed consent procedure approved by the Institutional Review Board at the University of Pennsylvania in accordance with the Declaration of Helsinki. All participants were previously analyzed in (Burke et al., 2022).

2.2. T1-weighted acquisition and preprocessing

High resolution T1-weighted MRI imaging was available for each of the 63 patients and 170 controls of the study. All images passed visual quality control (QC), performed by two independent, experienced raters

Table 1
Demographic characteristics of participants. SD = standard deviation, FTLD-tau = frontotemporal lobar degeneration due to tau, FTLD-TDP = FTLD due to TDP, MMSE = Mini mental state examination, *=significant difference between controls and FTLD-tau and controls and FTLD-TDP by *t*-test $p < 0.05$, ^=significant difference in proportion of males and females between controls and FTLD-tau.

	Controls	FTLD-tau	FTLD-TDP
N (female)^	167 (102)	42 (15)	21 (11)
Age At MRI (SD)	64.1 (8.41)	66.5 (7.62)	61.9 (9.16)
MMSE (SD)*	29.1 (0.89)	24.3 (4.61)	18.9 (8.65)
Education (SD)	15.6 (2.53)	16.2 (2.53)	15.6 (3.17)
Disease duration at MRI (SD)	N/A	4.73 (2.86)	3.38 (2.26)
MRI-autopsy interval (SD)	N/A	3.26 (2.00)	3.33 (2.48)

(CAO, SEB). Common reasons for failed QC were excessive head motion or poor segmentation. For additional details on pulse sequences, image processing, and quality control, please refer to (Burke et al., 2022). In the relatively rare case that we had multiple images for an individual pass QC, we selected the earliest available image, as it is the earliest phases of disease that are more difficult to discern yet are the most meaningful regarding impact on inclusion and likely benefit in treatment trials. All images were magnetization prepared rapid acquisition gradient echo (MPRAGE) acquired on Siemens scanners. T1-weighted images were processed using antsCorticalThickness.sh (Tustison et al., 2014). Briefly, the pipeline uses Advanced Normalization Tools (ANTs) to process the images, including N4 bias correction (Tustison et al., 2010), diffeomorphic registration from native space to template space, and Atropos brain segmentation (Avants et al., 2011) to identify cortex. To determine regional brain volumes, we used the cortical subset of the publicly available Lausanne parcellation with 250 labels per hemisphere (Hagmann et al., 2008). The native-template warps were used to transform the labels to each individual's native space.

2.3. W-score calculation

Cortical volumes were calculated in each ROI for each participant. To account for known differences in volume associated with age and intracranial volume, W-scores were used (La Joie et al., 2012). Briefly, W-scores use linear regression to remove the effect of confounding variables on a measurement of interest, and the standard deviation across samples is used to normalize variance across different ROIs in the data set; the process is similar to calculating a z-score but with covariates of no interest removed. For details on the W-score calculation procedure, please see (Burke et al., 2022; La Joie et al., 2012). We used the available healthy control data to generate W-scores at each ROI for each patient and healthy control. The equation generated from the control data was then applied to each data set for both healthy controls and patients. Due to consistently outlying W-score values, three additional controls with borderline visual QC were excluded.

2.4. Biomarker generation for EBM

EBM requires a set of biomarkers as input to become the change events, which are placed in the most likely or "characteristic" order. EBM requires more participants than biomarkers, and we wanted to verify that a machine learning method could create biomarkers related to pathologic burden at autopsy. We used the kmeans() function from the "stats" package in R (MacQueen, 1967; R Core Team, 2021) to perform two K-means clustering processes: one using as input the cortical volume w-scores of the FTLD-tau patients, and the other using cortical volume w-scores of the FTLD-TDP patients. To select the number of clusters to use in our EBM analysis, we used a combination of quantitative recommendation and biological hypotheses: we performed K-means clustering using one to 25 clusters and examined both the within cluster sum of squares (WCSS) and Akaike information criterion (AIC) for each number of clusters. Using the "elbow" method, both WCSS and AIC indicated the optimal number of clusters to be around five for each of our FTLD-tau and FTLD-TDP groups. We then calculated the mean w-score of the collection of ROIs from within each cluster for each of the FTLD-tau participants and each of the controls with the FTLD-tau clusters, and once for the FTLD-TDP participants and each of the controls with the FTLD-TDP clusters. In such a way, the large number of ROIs from the Lausanne 250 scale is sufficiently reduced to a reasonable number of biomarkers for each EBM: five.

2.5. EBM

EBM is a data-driven analysis technique that generates a likely sequence of events, using frequencies of deviations from a control group (Fonteijn et al., 2012). To perform EBM, we used the publicly available ebm package from GitHub (https://github.com/ucl-pond/ebm). Briefly, EBM assumes a set of change events is preserved across a patient group and that an ordering of these events exists. The set of events is determined by the biomarkers given to the model as input. For each analysis, one for FTLD-tau, and a second for FTLD-TDP, each patient and control has five biomarkers: one for each cluster of cortical volumes. As described above, each biomarker is the mean W-score of the ROIs from each identified cluster. Two key underlying assumptions in EBM are that biomarkers change monotonically and that all patients follow the same event sequence. This means that a participant cannot have a biomarker revert to an earlier phase once the event has occurred (i.e., a patient cannot return to "control" status). The structural MRI data sets of FTLD participants are thus good models for EBM, as cortical atrophy is thought to be irreversible over the course of neurodegeneration. Furthermore, all participants in each pathology group share a pathology that has been shown to share imaging features for early changes (Burke et al., 2022), which indicates that the patients within a pathology group are likely to follow the same sequence of events for early changes. Under such assumptions, a Markov Chain Monte Carlo (MCMC) model may be used to estimate the order of each event. However, MCMC requires a good prior sequence estimate to assure good fits in reasonable time, so a greedy ascent algorithm is used for initialization. The model begins by assuming each order is equally likely and proceeds to randomly switch pairs of events and estimate the likelihood of the data given the switched order. If the likelihood of the switched order is greater than the pre-switched order, the switched order becomes the new estimate. If the likelihood of the switched order is less than the likelihood of the pre-switched order, the pre-switched order is maintained as the estimate, and a new pair of events is switched. The simulation continues until a prespecified number of iterations is reached ($n = 2000$). To increase the likelihood that the true maximum likelihood is reached, different initialization points for the greedy algorithm are used ($n = 10$). After the optimal greedy estimate is determined, the MCMC simulation begins, initialized with the maximum likelihood greedy estimate, which is refined in a similar iterative event-pair-switching manner, until the specified number of iterations is reached ($n = 500{,}000$). Importantly, during the MCMC, the probabilities of each simulated sequence are remembered. In such a way, both the characteristic event ordering and positional variance calculations are preserved. The positional variance can then be examined to infer confidence in the model. For each biomarker, a Gaussian mixture model is used to determine the likelihood of the data given the events, as in (Fonteijn et al., 2011). The Gaussian mixture model was used, as opposed to a uniform distribution, as we expected approximately normal distributions of measurements for each biomarker. Furthermore, the EBM was then used to estimate where in the sequence of events each participant is, giving each participant a disease stage or "disease severity" estimate.

In such a way, two EBM procedures were run. The first with the five mean W-scores of the cortical volumetric FTLD-tau cluster biomarkers for the patients with FTLD-tau and control participants, and the second for the five mean W-scores of the cortical volumetric FTLD-TDP cluster biomarkers for the patients with FTLD-TDP and control participants. Each EBM model generates a characteristic sequence and positional variance diagram for the group of participants, as well as a stage estimate for each participant. The characteristic sequences of the EBM analysis can be examined to determine the likely order of cortical volume changes for the two groups. The positional variance diagrams can also be examined to infer confidence about each characteristic sequence. The per-patient stage estimates based upon volumes can be used to probe associations with other disease metrics, such as pathologic burden or cognition (see below). To examine whether pathological subtypes influenced EBM-estimated stages, two ANOVAs were run comparing EBM-estimated stages within each "umbrella" of FTLD-tau and FTLD-TDP. Post-hoc t-tests were used to probe which subtypes were significantly different, if any. All results were considered significant at $p < 0.05$ (uncorrected for multiple comparisons).

2.6. Pathologic burden and estimated stage regressions

Pathology is the "gold standard" for diagnosis of FTLD-tau and FTLD-TDP. It is important that *in vivo* biomarkers of disease severity, such as estimated stage from EBM, are validated against this gold standard. For most participants, we studied burden of pathology from a random hemisphere at autopsy according to standardized NIA/AA diagnostic guidelines (Hyman et al., 2012) in a group of consistently-sampled regions (see below) in autopsied patients. Bilateral sampling was done in a small subset of patients, and measurements from regions sampled bilaterally were averaged together within a patient. The available number of patient autopsy samples in each group included: the anterior cingulate (aCING: number with FTLD-tau = 26, FTLD-TDP = 15), middle frontal cortex (MFC, FTLD-tau = 28, FTLD-TDP = 15), orbitofrontal cortex (OFC, FTLD-tau = 29, FTLD-TDP = 14), superior-middle temporal cortex (SMTC, FTLD-tau = 29, FTLD-TDP = 14), angular gyrus (ANG, FTLD-tau = 23, FTLD-TDP = 14). Briefly, tissue was fixed in 10 % formalin and immunostained for tau (AT8; Invitrogen) (Mercken et al., 1992) or phosphorylated TDP-43 (rat monoclonal TAR5P-1D3; Millipore Sigma) (Neumann et al., 2009) and then an Aperio AT2 (Leica Biosystem, Wetzlar, Germany) was used to obtain 20x magnification whole-slide images (Giannini et al., 2019a; Irwin et al., 2016a). QuPath software version 0.3.0 (Bankhead et al., 2017) was used to measure the percent area occupied (%AO) of FTLD-tau or FTLD-TDP inclusions in GM in each slide (Giannini et al., 2019b; Irwin et al., 2016a). Each EBM produces a single estimate of each participant's disease stage that is based upon a distributed network of brain regions. Thus, we wanted a similarly distributed estimate of pathologic burden for each patient. To achieve this, we began by log-transforming the %AO in each of the regions listed above to account for the skewed distribution of this measurement (Burke et al., 2022; Giannini et al., 2019b). Finally, to obtain one total score for pathologic burden per patient, we took the arithmetic mean of the log %AO data for the above-mentioned regions for each patient so we could relate this to the EBM-estimated stage (see below).

We tested the relationships between EBM-estimated stage for each patient and pathologic burden. To do so, we performed linear regression analyses, using the summarized quantitative pathologic burden as the dependent variable. We attempted to correct for multiple comparisons but found only significant results with FTLD-TDP in this relatively small sample, so we report uncorrected results using a reasonable threshold for significance, $p < 0.05$ (uncorrected).

2.7. Cognitive impairment and estimated stage regressions

To determine whether the EBM-estimated stage for each patient is clinically informative, the EBM-estimated stages were investigated in subsets of patients with an available measure of general cognition: MMSE (FTLD-tau = 40, FTLD-TDP = 17). Similar to the pathologic burden analysis, we performed linear regression analyses to test the relationships between the measure of cognition (dependent variable) and EBM-estimated stage for each patient with available data (independent variable), considering results significant at $p < 0.05$ (uncorrected).

3. Results

3.1. K-means clusters

K-means clustering was used twice, once to create five clusters of regions to be used as biomarkers for FTLD-tau EBM, and once to create five clusters of regions to be used as biomarkers for FTLD-tau EBM. Panel A of Fig. 1 shows the clusters for FTLD-tau, with one cluster representing mostly bilateral frontal cortex, with some temporal regions included (orange), one bilateral anterior temporal and insular cluster that also includes orbitofrontal cortex (yellow), one cluster that includes much parietal cortex, with some temporal and frontal cortex as well (dark red),

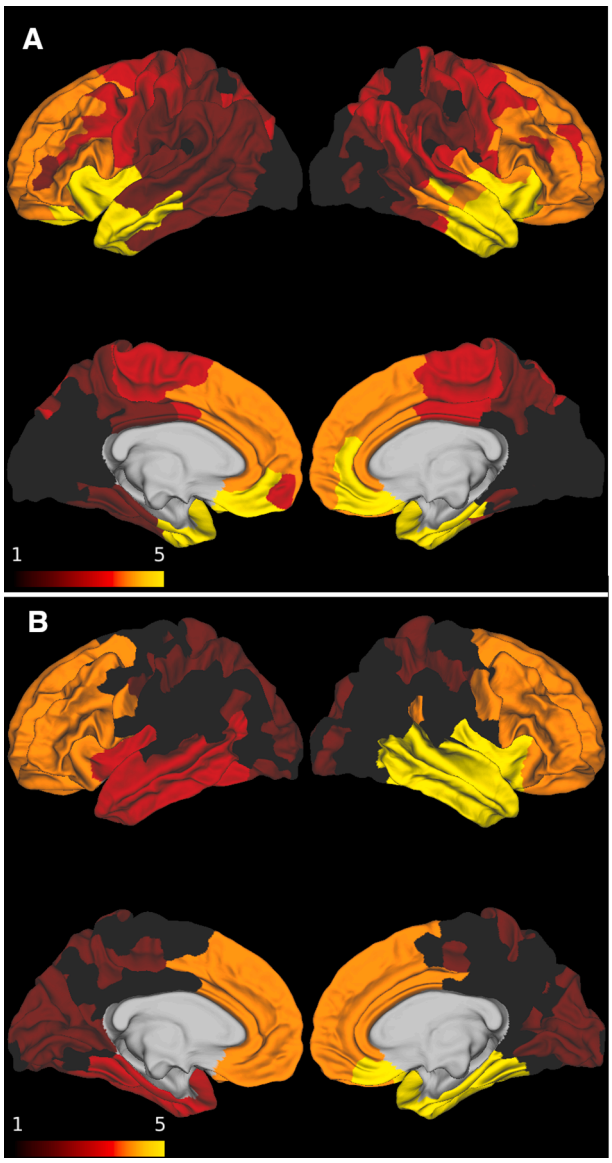

Fig. 1. K-means clusters of cortical volumes for A) FTLD-tau and B) FTLD-TDP.

a cluster that encompasses much of the bilateral motor and supplementary motor cortex, in addition to some frontal and parietal cortex (bright red), and finally a majority occipital cluster, that also includes some parietal cortex (black).

FTLD-TDP results in somewhat different clusters, as shown in Fig. 1. B. One cluster nearly encompasses left temporal lobe and insula (bright red), with another relatively symmetric cluster on the right side (yellow). There's also a bilateral frontal cluster (orange). The remaining two clusters cover the parietal and occipital cortex, with one covering the precentral gyrus, much of the angular gyrus and other parietal and occipital cortex (black) and finally a cluster covering most of the occipital pole and medial occipital cortex, along with some superior parietal cortex (dark red).

3.2. EBM of FTLD-tau and FTLD-TDP

To test whether the data-driven EBM can determine a meaningful sequence of machine learning-based biomarkers, we used the five cortical volume biomarkers for each patient group generated by K-means clustering in an EBM analysis for the respective patient groups relative to the same set of controls. Note that the only information about

the biomarkers given to EBM was the study group in which they belonged (control "0" vs patient "1"), and EBM then determines their most likely or "characteristic" sequence order. As shown in Fig. 2.A, results of the cortical volumetric FTLD-tau EBM were assigned the characteristic sequence occipital, motor, parietal, then frontal, and finally temporal. The motor and parietal events show some positional variance, though variance is low for the other three events.

The FTLD-TDP EBM generates a characteristic sequence as shown in Fig. 2.B. Similar to FTLD-tau, events 1 and 2 are the clusters with posterior regions, beginning with the parietal and occipital clusters. Left temporal, bilateral frontal, and right temporal clusters are the next events, respectively, and they demonstrate relatively low positional variance.

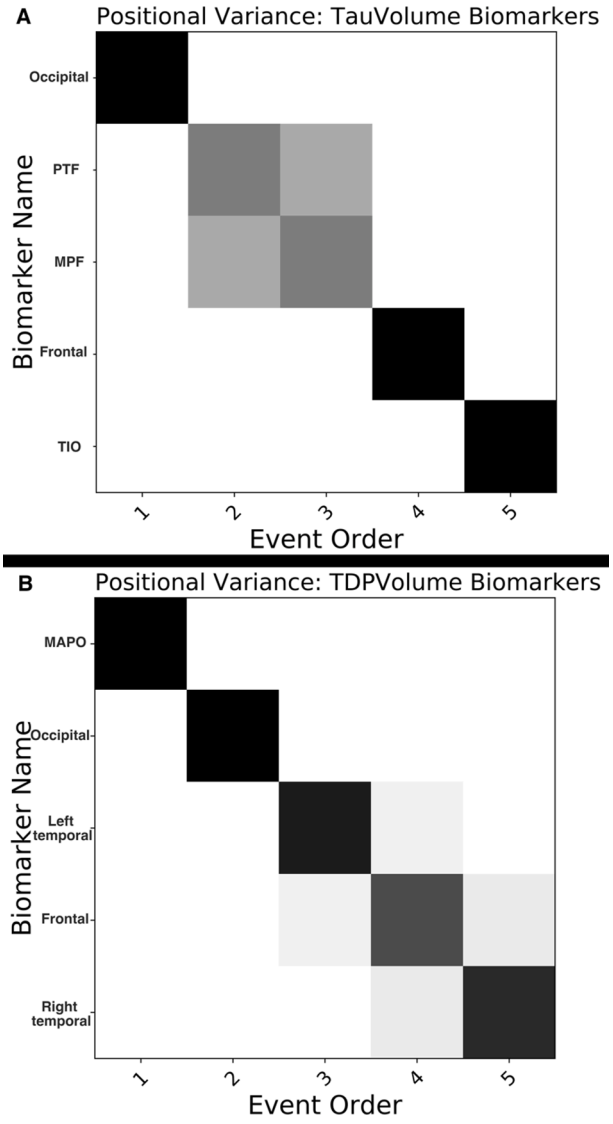

Fig. 2. Characteristic sequence from event-based models (EBM). Event order is the characteristic sequence generated by running EBM. Biomarkers are the mean W-scores from all ROIs within each disease cluster. The grayscale in each row represents confidence of placement of that biomarker in that place in the event order, with darker hues representing higher confidence in the event placement, and lighter representing lower confidence. A. The FTLD-tau data EBM characteristic sequence. Positional variance is low for events 1 (occipital; black in Fig. 1.A), 4 (frontal; orange), and 5 (temporal, insula, orbitofrontal (TIO); yellow), the motor, parietal, frontal (MPF; bright red) and parietal, temporal and frontal (PTF; dark red) events show some variance. B. The FTLD-TDP EBM generates a characteristic sequence of the motor, angular, parietal and occipital (MAPO; black in Fig. 1.B) cluster followed by the occipital cluster (dark red), with left temporal (bright red) next, followed by frontal (orange), and finally right temporal (yellow) events. There is relatively low positional variance in the FTLD-TDP sequence, with some present between the left temporal, bilateral frontal, and right temporal events.

The ANOVA comparing EBM-estimated stages across isoforms of FTLD-tau were significant ($p = 0.003$, $f(2, 39) = 6.65$). Post-hoc t-tests showed that, PiD tended to have higher estimated stages than CBS ($p = 0.0009$, $t(19) = 3.95$) and PSP ($p = 0.0001$, $t(27) = 4.37$). For FTLD-TDP, there was no significant effect of isoform on EBM-estimated stage ($p = 0.062$).

3.3. Pathologic burden and estimated stage regressions

EBM also produced an estimate for the stage of each patient based upon their biomarkers. As the biomarkers indicate the extent of disease, this EBM-estimated stage is a proxy of disease severity. A low estimated stage (e.g. 1 or 2) indicates change having occurred only in one or relatively few biomarkers in the characteristic sequence. Greater EBM-estimated stages (e.g. 4 or 5) indicates patients with more widespread cortical atrophy and typically including atrophy in all of the preceding stages. To verify whether more severe disease stage estimates, derived from the five volumetric biomarkers for each patient, were associated with greater pathologic burden in FTLD-tau and FTLD-TDP, we performed linear regressions with the EBM-estimated stage as the independent variable and the pathologic burden the dependent variable. The estimated volumetric stage was significantly positively associated with pathologic burden, meaning that a greater extent of cortical volume loss, represented by a later volumetric stage, was associated with greater pathologic burden in FTLD-tau ($R^2 = 0.16$, $t(1, 28) = 2.55$, $p = 0.017$; see Fig. 3.A). The EBM-estimated stage also demonstrated a significant association with pathologic burden in FTLD-TDP ($R^2 = 0.51$, $t(1, 15) = 4.19$, $p = 0.0008$; see Fig. 3.B). As interval between MRI and autopsy may modulate the relationship between EBM-estimated stage and pathologic burden within an individual, regressions were also run with MRI-autopsy interval as a covariate, but results remained similar.

3.4. Cognitive impairment and estimated stage regressions

To determine whether more severe disease estimated by EBM analysis of T1 volumetric imaging was associated with worse cognition, we performed linear regression analysis similar to the one described above, but with MMSE as the dependent variable, and again estimated stage as the independent variable. Patients did not demonstrate a significant association between EBM-estimated stages and MMSE for either FTLD-tau or FTLD-TDP groups ($p > 0.05$).

4. Discussion

We applied EBM to MRI data of autopsy-confirmed patients with FTLD-tau and FTLD-TDP. Based on AIC and WCSS, K-means clustering suggested five clusters for cortical MRI volumetric biomarkers for patients with FTLD-tau and FTLD-TDP. Using these clusters as input, EBM generated a statistically robust solution for ordering these clusters as events in each pathology group. EBM thus determined that the characteristic sequence of cortical volume biomarker change events for each of FTLD-tau and FTLD-TDP. The EBM-estimated stage for each patient *in vivo* was related to quantitative digital measures of pathology found at autopsy in each group using linear regression. These results indicate the ability of EBM to capture and model *in vivo* imaging for the purpose of identifying the accumulation of pathologic inclusions of both FTLD-tau and FTLD-TDP. Thus, we have indicated that EBM can meaningfully inform patients' disease state relative to the gold standard of pathology. We discuss each of these aspects of our study below.

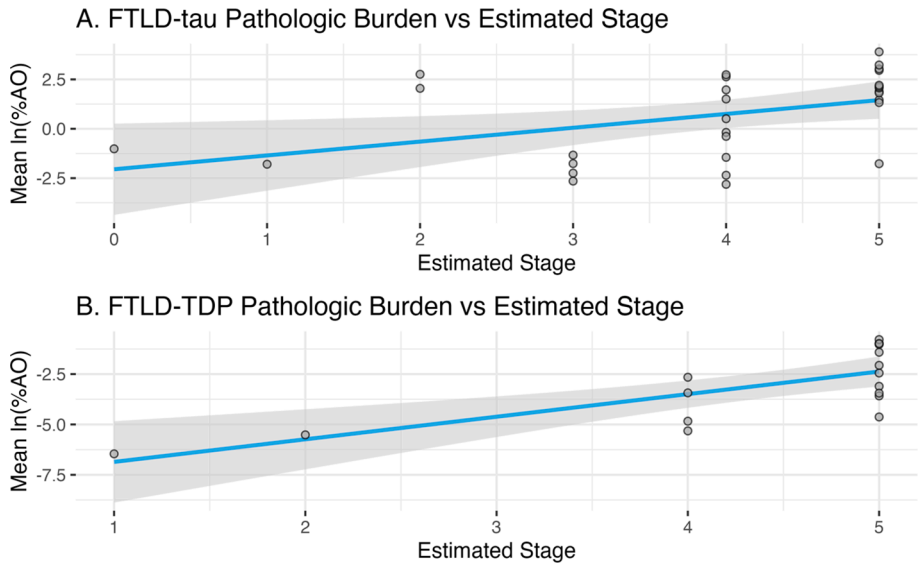

Fig. 3. Event-based modeling (EBM)-estimated stage regressions. A. EBM-estimated stage based upon cortical volumes display a significant positive relationship with pathologic burden in patients with FTLD-tau, summarized as the mean log percent area occupied (ln(%AO); $p = 0.017$). B. EBM-estimated stage derived from cortical volumes in patients with FTLD-TDP also demonstrate a significant relationship with pathologic burden ($p = 0.0008$).

4.1. K-means of FTLD-tau and FTLD-TDP

In patients with neurodegenerative disease that results in cortical volume loss, such as those with FTLD-tau and FTLD-TDP, K-means clustering identifies anatomic regions with similar amounts of cortical atrophy and groups them into clusters. In FTLD-tau and FTLD-TDP, the created clusters follow a somewhat expected pattern (Brettschneider et al., 2014; Irwin et al., 2016a; Irwin et al., 2016b; Seeley et al., 2008; Whitwell et al., 2007, Whitwell et al., 2011). FTLD-tau clusters are largely symmetric bilaterally, and while three of the five clusters in FTLD-TDP are bilaterally symmetric, the final two clusters each encompass one temporal lobe. This may be due to a preponderance of patients with the semantic variant of primary progressive aphasia (svPPA) in this group (Hodges et al., 1992), where atrophy is more prominent in the left temporal lobe than the right temporal lobe. Though generated using data from the same patients as the atrophy phases published in (Burke et al., 2022), the K-means clusters for both patient groups are distinct from these phases. This difference is likely due to the different methodological techniques used to capture disease: establishing an arbitrarily low threshold for atrophy, as in (Burke et al., 2022), may increase sensitivity to the earliest phases of disease in some regions, but by clustering regions objectively statistical power is improved.

K-means is a simple, interpretable, and fast unsupervised clustering method. When applied to structural cortical volume data, it provides immediately interpretable cluster of regions which can be grouped together to form biomarkers for other algorithms, like EBM. While PCA is another unsupervised machine learning method that is both simple and fast, the clusters that PCA creates are a linear combination of the original data; in the context of cortical volumes, this makes interpretation difficult as regions are likely to partially participate in multiple different clusters. Furthermore, the PCA transformed results can be signed, which can also muddy interpretation. K-means also has some drawbacks, including requiring a specified number of unique clusters, its sensitivity to noise, and a tendency to perform best when clusters are of a similar size, all of which may potentially be of some concern when considering analysis of cortical volume data. PCA and other similar methods that have begun to address the concerns related to its application to brain data should be considered in future work (Avants et al., 2014; Zuendorf et al., 2003).

4.2. EBM in FTLD-tau and FTLD-TDP

This study demonstrates both strengths and weaknesses of EBM. Strengths include interpretability of both the sequence of events and confidence in the sequence, as shown by EBM calculating both the characteristic sequence and its positional variance. In EBM, the earliest regions in the characteristic sequences - in this study, events labeled 4 and 5 in Fig. 2 – identify the earliest loci of pathology or "epicenters". Later regions in the sequence of events – in this study, events labeled 1 and 2 – are regions affected later in the disease course. While initial studies of EBM used longitudinal data (Fonteijn et al., 2012; Young et al., 2014), the present study examines cross-sectional cohorts of patients, so interpretability is somewhat more nuanced as we are not examining changes, but ordered snapshots of disease based on volumes of cortical atrophy where each subsequent stage encompasses earlier stages. Thus, that both the FTLD-tau and FTLD-TDP characteristic sequences represent a likely pattern of least to most pathology makes some sense. The "early" events in FTLD-tau, changes in the frontal and temporal lobes, are consistent measurements in patients, as determined by their extremely low positional variance. The later events, changes in the parietal and motor regions, demonstrate more positional variance, as it is possible that as different FTLD-tau isoforms show some phenotypic differences reflected in later disease stages (Burke et al., 2022; Josephs et al., 2008; Whitwell et al., 2011; Whitwell et al., 2009b). Finally, the occipital lobe is perhaps minimally affected in most patients, again showing extremely low positional variance. Similarly for FTLD-TDP, temporal and frontal regions demonstrate the most pathology, and parietal and occipital regions relatively less so. These ordered stages of disease are also seen in pathologic assessments of FTLD-tau (Irwin et al., 2016a; Kovacs et al., 2020) and FTLD-TDP (Brettschneider et al., 2013, Brettschneider et al., 2014).

The individual patient EBM-estimated stage measurements are an important feature of EBM as well. Though past studies of EBM and similar methods have associated estimated stage with follow-up EBM stage, clinical diagnosis, or the contralateral homologue measurements in neurodegenerative diseases (Panman et al., 2021; Young et al., 2014), this is the first study to show that the EBM-estimated disease stage is related to underlying pathological burden. This is important as pathology remains the "gold standard" for disease in FTLD. We showed a predictive relationship between a distributed antemortem measure of brain structure and a similarly distributed representative sample tissue

measure of pathologic burden in each of FTLD-tau and FTLD-TDP. This relationship provides converging evidence with past studies examining associations between structural imaging measures and pathologic burden (Burke et al., 2022; Giannini et al., 2019a; Irwin et al., 2016a; Whitwell et al., 2009a). Though MMSE is regularly shown to be impaired in patients with FTLD and worsens over time (Bian et al., 2008; Cousins et al., 2021; Tan et al., 2013), we did not find such an association. This may be due in part to the fact that the MMSE was originally developed to monitor overall clinical change in AD patients with memory difficulty, and future work should perhaps examine EBM-estimated stages measures that are potentially more specific for FTLD, such as automated speech measures or the Philadelphia Brief Assessment of Cognition (PBAC) (Cho et al., 2021; Cousins et al., 2021; Libon et al., 2011; Nevler et al., 2019).

4.3. Limitations

Though the results are promising, the current study has some shortcomings. First, because FTLD is a rare condition, imaging studies in these rare cases are quite uncommon, and imaging studies of autopsy-proven cases of FTLD-tau and FTLD-TDP are even rarer, therefore the number of participants is relatively small, particularly those with FTLD-TDP. There are different isoforms of FTLD-tau, primarily Pick's disease (PiD), progressive supranuclear palsy (PSP), and corticobasal degeneration (CBD), and FTLD-TDP has types A, B, C, and E. While neuropathological staging studies of PiD and a heterogeneous cohort of FTLD-tau pathology suggest that PiD is likely to display early pathology in cortex (Irwin et al., 2016a; Irwin et al., 2018), a similar study examining pathology in PSP emphasized subcortical structures, which we were not able to examine here, though pathology was also present in cortex (Kovacs et al., 2020). As such, subcortical structures should also be examined in EBM studies adequately powered to analyze isoforms of FTLD-tau (Irwin et al., 2016a; Kovacs et al., 2020). While we found no significant differences in EBM-estimated stage between isoforms of FTLD-TDP, this may be due to the relatively small sample sizes for each subgroup (Mackenzie & Neumann, 2016). Thus, a shortcoming of the present work is that the study is underpowered to use EBM to examine phases in the subgroups of patients with FTLD-TDP separately, and this should be a direction for future research. As with any data-driven analysis method, validating results on an independent cohort should be a direction for future work, though, as mentioned, there are relatively few available FTLD patient datasets with both MRIs and regional pathology data. Though we found an association between cortical volume EBM-estimated stage and pathologic burden, this was found to be significant only when not correcting for multiple comparisons for the different regressions we performed with this rare cohort of patients. Furthermore, though EBM-estimated stages are associated with pathologic burden for both FTLD-tau and FTLD-TDP, the characteristic sequences may not map onto expected patterns based upon existing pathology literature. This may be due in part to the relatively sparse pathology sampling representing much less than the full brain coverage available from MRI metrics. K-means is a relatively simple clustering method and other clustering methods with sparsity and anatomical adjacency constraints may warrant consideration in the future (Avants et al., 2014; Cook et al., 2014; Kandel et al., 2015). EBM has the potential to incorporate longitudinal data, but the present study was underpowered to explore this possibility. Another strength of EBM is its ability to seamlessly integrate multiple modalities, such as both structural and functional imaging measures. Some studies have indicated that hypoperfusion may precede structural changes in FTLD (Dopper et al., 2016; Ferraro et al., 2018; Olm et al., 2016) and that MRI perfusion is a candidate for monitoring longitudinal changes in FTLD (Ssali et al., 2022), so future studies should examine EBM in the context of longitudinal multimodal imaging studies in pathology-confirmed FTLD patients.

5. Conclusions

EBM is a promising machine learning tool for understanding neurodegenerative disease progression *in vivo*. We've shown that EBM of volumetric cortical data derived from MRI can produce results that parallel those from autopsy studies. Individual patient EBM-estimated stages are associated with digitally quantified pathologic burden, validating the utility of EBM in capturing signal related to the important underlying biology in both FTLD-tau and FTLD-TDP. This connection should encourage future work using EBM as an *in vivo* method for monitoring disease modifying treatments in neurodegenerative disorders.

CRediT authorship contribution statement

Christopher A. Olm: Conceptualization, Methodology, Software, Validation, Formal analysis, Investigation, Data curation, Writing – original draft, Writing – review & editing, Visualization. **Sarah E. Burke:** Investigation, Data curation, Writing – review & editing, Data curation, Writing – review & editing. **Claire Peterson:** Methodology, Software, Investigation. **Edward B. Lee:** Investigation, Resources, Data curation, Writing – review & editing, Funding acquisition. **John Q. Trojanowski:** Investigation, Resources, Data curation, Writing – review & editing, Funding acquisition. **Lauren Massimo:** Investigation, Resources, Data curation, Writing – review & editing, Funding acquisition. **David J. Irwin:** Methodology, Software, Formal analysis, Investigation, Resources, Writing – review & editing, Funding acquisition. **Murray Grossman:** Conceptualization, Methodology, Investigation, Resources, Writing – review & editing, Supervision, Funding acquisition. **James C. Gee:** Conceptualization, Methodology, Resources, Writing – review & editing, Supervision, Funding acquisition.

Declaration of Competing Interest

The authors declare that they have no known competing financial interests or personal relationships that could have appeared to influence the work reported in this paper.

Data availability

Data will be made available on request.

Acknowledgements

This work was supported by the National Institutes of Health [grant numbers AG066597, AG052943, NS109260, AG061277, AG054519, AG072979, AG062418]. The funding sources were not involved in the collection, analysis and interpretation of data, in the writing of the report, or in the decision to submit the article for publication. The authors sincerely appreciate the study participants, especially patients and their families, without whom the research would not be possible.

References

Avants, B.B., Tustison, N.J., Wu, J., Cook, P.A., Gee, J.C., Wu, J., Cook, P.A., Gee, J.C., 2011. An open source multivariate framework for n-tissue segmentation with evaluation on public data. Neuroinformatics 9 (4), 381–400. https://doi.org/10.1007/s12021-011-9109-y.

Avants, B.B., Libon, D.J., Rascovsky, K., Boller, A., McMillan, C.T., Massimo, L., Coslett, H.B., Chatterjee, A., Gross, R.G., Grossman, M., 2014. Sparse canonical correlation analysis relates network-level atrophy to multivariate cognitive measures in a neurodegenerative population. Neuroimage 84, 698–711. https://doi.org/10.1016/j.neuroimage.2013.09.048.

Bankhead, P., Loughrey, M.B., Fernández, J.A., Dombrowski, Y., McArt, D.G., Dunne, P. D., McQuaid, S., Gray, R.T., Murray, L.J., Coleman, H.G., James, J.A., Salto-Tellez, M., Hamilton, P.W., 2017. QuPath: Open source software for digital pathology image analysis. Sci. Rep. 7 (1), 1–7. https://doi.org/10.1038/s41598-017-17204-5.

Bian, H., Van Swieten, J.C., Leight, S., Massimo, L., Wood, E., Forman, M., Moore, P., de Koning, I., Clark, C.M., Rosso, S., Trojanowski, J., Lee, V.M.-Y., Grossman, M., 2008. CSF biomarkers in frontotemporal lobar degeneration with known pathology. Neurology 70 (19, Part 2), 1827–1835.

Brettschneider, J., Del Tredici, K., Toledo, J.B., Robinson, J.L., Irwin, D.J., Grossman, M., Suh, E., Van Deerlin, V.M., Wood, E.M., Baek, Y., Kwong, L., Lee, E.B., Elman, L., McCluskey, L., Fang, L., Feldengut, S., Ludolph, A.C., Lee, V.-M.-Y., Braak, H., Trojanowski, J.Q., 2013. Stages of pTDP-43 pathology in amyotrophic lateral sclerosis. Ann. Neurol. 74 (1), 20–38. https://doi.org/10.1002/ana.23937.

Brettschneider, J., Del Tredici, K., Irwin, D.J., Grossman, M., Robinson, J.L., Toledo, J.B., Fang, L., Van Deerlin, V.M., Ludolph, A.C., Lee, V.M.Y., Braak, H., Trojanowski, J.Q., 2014. Sequential distribution of pTDP-43 pathology in behavioral variant frontotemporal dementia (bvFTD). Acta Neuropathol. 127 (3), 423–439. https://doi.org/10.1007/s00401-013-1238-y.

Burke, S.E., Phillips, J.S., Olm, C.A., Peterson, C.S., Cook, P.A., Gee, J.C., Lee, E.B., Trojanowski, J.Q., Massimo, L., Irwin, D.J., Grossman, M., 2022. Phases of volume loss in patients with known frontotemporal lobar degeneration spectrum pathology. Neurobiol. Aging 113, 95–107. https://doi.org/10.1016/j.neurobiolaging.2022.02.007.

Capozzo, R., Sassi, C., Hammer, M.B., Arcuti, S., Zecca, C., Barulli, M.R., Tortelli, R., Gibbs, J.R., Crews, C., Seripa, D., Carnicella, F., Dell'Aquila, C., Rossi, M., Tamma, F., Valluzzi, F., Brancasi, B., Panza, F., Singleton, A.B., Logroscino, G., 2017. Clinical and genetic analyses of familial and sporadic frontotemporal dementia patients in Southern Italy. Alzheimer's & Dementia 13 (8), 858. https://doi.org/10.1016/J.JALZ.2017.01.011.

Cho, S., Nevler, N., Ash, S., Shellikeri, S., Irwin, D.J., Massimo, L., Rascovsky, K., Olm, C., Grossman, M., Liberman, M., 2021. Automated analysis of lexical features in frontotemporal degeneration. Cortex 137, 215–231. https://doi.org/10.1016/j.cortex.2021.01.012.

Cook, P.A., McMillan, C.T., Avants, B.B., Peelle, J.E., Gee, J.C., Grossman, M., 2014. Relating brain anatomy and cognitive ability using a multivariate multimodal framework. Neuroimage 99, 477–486. https://doi.org/10.1016/j.neuroimage.2014.05.008.

Cousins, K.A.Q., Bove, J., Giannini, L.A.A., Kinney, N.G., Balgenorth, Y.R., Rascovsky, K., Lee, E.B., Trojanowski, J.Q., Grossman, M., Irwin, D.J., 2021. Longitudinal naming and repetition relates to AD pathology and burden in autopsy-confirmed primary progressive aphasia. Alzheimer's and Dementia: Transl. Res. Clin. Intervent. 7 (1), 1–10. https://doi.org/10.1002/trc2.12188.

Dopper, E.G.P., Chalos, V., Ghariq, E., den Heijer, T., Hafkemeijer, A., Jiskoot, L.C., de Koning, I., Seelaar, H., van Minkelen, R., van Osch, M.J.P., Rombouts, S.A.R.B., van Swieten, J.C., 2016. Cerebral blood flow in presymptomatic MAPT and GRN mutation carriers: A longitudinal arterial spin labeling study. NeuroImage: Clinical 12 (016130677), 460–465. https://doi.org/10.1016/j.nicl.2016.08.001.

Ferraro, P.M., Jester, C., Olm, C.A., Placek, K., Agosta, F., Elman, L., McCluskey, L., Irwin, D.J., Detre, J.A., Filippi, M., Grossman, M., McMillan, C.T., 2018. Perfusion alterations converge with patterns of pathological spread in transactive response DNA-binding protein 43 proteinopathies. Neurobiol. Aging 68, 85–92. https://doi.org/10.1016/j.neurobiolaging.2018.04.008.

Fonteijn, H. M., Clarkson, M. J., Modat, M., Barnes, J., Lehmann, M., Ourselin, S., Fox, N. C., & Alexander, D. C. (2011). An Event-Based Disease Progression model and its application to familial Alzheimer's Disease. *Biennial International Conference on Information Processing in Medical Imaging*, 1–12. http://link.springer.com/chapter/10.1007/978-3-642-22092-0_61.

Fonteijn, H.M., Modat, M., Clarkson, M.J., Barnes, J., Lehmann, M., Hobbs, N.Z., Scahill, R.I., Tabrizi, S.J., Ourselin, S., Fox, N.C., Alexander, D.C., 2012. An event-based model for disease progression and its application in familial Alzheimer's disease and Huntington's disease. Neuroimage 60 (3), 1880–1889. https://doi.org/10.1016/j.neuroimage.2012.01.062.

Giannini, L.A.A., Xie, S.X., McMillan, C.T., Liang, M., Williams, A., Jester, C., Rascovsky, K., Wolk, D.A., Ash, S., Lee, E.B., Trojanowski, J.Q., Grossman, M., Irwin, D.J., 2019a. Divergent patterns of TDP-43 and tau pathologies in primary progressive aphasia. Ann. Neurol. 85 (5), 630–643. https://doi.org/10.1002/ana.25465.

Giannini, L.A.A., Xie, S.X., Peterson, C., Zhou, C., Lee, E.B., Wolk, D.A., Grossman, M., Trojanowski, J.Q., McMillan, C.T., Irwin, D.J., 2019b. Empiric methods to account for pre-analytical variability in digital histopathology in frontotemporal lobar degeneration. Front. Neurosci. 13 (JUL), 1–17. https://doi.org/10.3389/fnins.2019.00682.

Hagmann, P., Cammoun, L., Gigandet, X., Meuli, R., Honey, C. J., Wedeen, V. J., Sporns, O. (2008). Mapping the structural core of human cerebral cortex. *PLoS Biol.*, *6*(7), e159. https://doi.org/10.1371/journal.pbio.0060159.

Hodges, J.R., Patterson, K., Oxbury, S., Funnell, E., 1992. Semantic dementia: progressive fluent aphasia with temporal lobe atrophy. Brain 115 (6), 1783–1806. https://doi.org/10.1093/brain/115.6.1783.

Hyman, B.T., Phelps, C.H., Beach, T.G., Bigio, E.H., Cairns, N.J., Carrillo, M.C., Dickson, D.W., Duyckaerts, C., Frosch, M.P., Masliah, E., Mirra, S.S., Nelson, P.T., Schneider, J.A., Thal, D.R., Thies, B., Trojanowski, J.Q., Vinters, H.V., Montine, T.J., 2012. National Institute on Aging-Alzheimer's Association guidelines for the neuropathologic assessment of Alzheimer's disease. Alzheimer's Dementia 8 (1), 1–13. https://doi.org/10.1016/j.jalz.2011.10.007.

Irwin, D.J., Brettschneider, J., McMillan, C.T., Cooper, F., Olm, C., Arnold, S.E., Van Deerlin, V.M., Seeley, W.W., Miller, B.L., Lee, E.B., Lee, V.-M.-Y., Grossman, M., Trojanowski, J.Q., 2016a. Deep clinical and neuropathological phenotyping of Pick disease. Ann. Neurol. 79 (2), 272–287. https://doi.org/10.1002/ana.24559.

Irwin, D.J., Byrne, M.D., McMillan, C.T., Cooper, F., Arnold, S.E., Lee, E.B., Van Deerlin, V.M., Xie, S.X., Lee, V.M.Y., Grossman, M., Trojanowski, J.Q., 2016b. Semi-automated digital image analysis of Pick's disease and TDP-43 proteinopathy. J. Histochem. Cytochem. 64 (1), 54–66. https://doi.org/10.1369/0022155415614303.

Irwin, D.J., McMillan, C.T., Xie, S.X., Rascovsky, K., Van Deerlin, V.M., Coslett, H.B., Hamilton, R., Aguirre, G.K., Lee, E.B., Lee, V.-M.-Y., Trojanowski, J.Q., Grossman, M., 2018. Asymmetry of post-mortem neuropathology in behavioural-variant frontotemporal dementia. Brain 141 (1), 288–301. https://doi.org/10.1093/brain/awx319.

Janssen, J.C., Warrington, E.K., Morris, H.R., Lantos, P., Brown, J., Revesz, T., Wood, N., Khan, M.N., Cipolotti, L., Fox, N.C., Rossor, M.N., 2002. Clinical features of frontotemporal dementia due to the intronic tau 10+16 mutation. Neurology 58 (8), 1161–1168. https://doi.org/10.1212/WNL.58.8.1161.

Josephs, K.A., Whitwell, J.L., Dickson, D.W., Boeve, B.F., Knopman, D.S., Petersen, R.C., Parisi, J.E., Jack, C.R., 2008. Voxel-based morphometry in autopsy proven PSP and CBD. Neurobiol. Aging 29 (2), 280–289. https://doi.org/10.1016/j.neurobiolaging.2006.09.019.

Kandel, B.M., Wang, D.J., Gee, J.C., Avants, B.B., 2015. Eigenanatomy: sparse dimensionality reduction for multi-modal medical image analysis. Methods 43–53. https://doi.org/10.1007/s11103-011-9767-z.

Kovacs, G.G., Lukic, M.J., Irwin, D.J., Arzberger, T., Respondek, G., Lee, E.B., Coughlin, D., Giese, A., Grossman, M., Kurz, C., McMillan, C.T., Gelpi, E., Compta, Y., van Swieten, J.C., Laat, L.D., Troakes, C., Al-Sarraj, S., Robinson, J.L., Roeber, S., Xie, S.X., Lee, V.-Y., Trojanowski, J.Q., Höglinger, G.U., 2020. Distribution patterns of tau pathology in progressive supranuclear palsy. Acta Neuropathol. 140 (2), 99–119.

La Joie, R., Perrotin, A., Barré, L., Hommet, C., Mézenge, F., Ibazizene, M., Camus, V., Abbas, A., Landeau, B., Guilloteau, D., de La Sayette, V., Eustache, F., Desgranges, B., Chételat, G., 2012. Region-specific hierarchy between atrophy, hypometabolism, and 2-amyloid (Aβ) load in Alzheimer's disease dementia. J. Neurosci. 32 (46), 16265–16273. https://doi.org/10.1523/JNEUROSCI.2170-12.2012.

Libon, D.J., Rascovsky, K., Gross, R.G., White, M.T., Xie, S.X., Dreyfuss, M., Boller, A., Massimo, L., Moore, P., Kitain, J., Coslett, H.B., Chatterjee, A., Grossman, M., 2011. The Philadelphia Brief Assessment of Cognition (PBAC): validated screening measure for dementia. Clin. Neurophysiol. 25 (8), 1314–1330. https://doi.org/10.1080/13854046.2011.631585.

López, M., Ramírez, J., Górriz, J.M., Álvarez, I., Salas-Gonzalez, D., Segovia, F., Chaves, R., Padilla, P., Gómez-Río, M., 2011. Principal component analysis-based techniques and supervised classification schemes for the early detection of Alzheimer's disease. Neurocomputing 74 (8), 1260–1271. https://doi.org/10.1016/j.neucom.2010.06.025.

Mackenzie, I.R.A., Neumann, M., 2016. Molecular neuropathology of frontotemporal dementia: insights into disease mechanisms from postmortem studies. J. Neurochem. 138, 54–70. https://doi.org/10.1111/jnc.13588.

Mackenzie, I.R.A., Neumann, M., Bigio, E.H., Cairns, N.J., Alafuzoff, I., Kril, J., Kovacs, G.G., Ghetti, B., Halliday, G., Holm, I.E., Ince, P.G., Kamphorst, W., Revesz, T., Rozemuller, A.J.M., Kumar-Singh, S., Akiyama, H., Baborie, A., Spina, S., Dickson, D.W., Trojanowski, J.Q., Mann, D.M.A., 2009. Nomenclature for neuropathologic subtypes of frontotemporal lobar degeneration: consensus recommendations. Acta Neuropathol. 117 (1), 15–18.

Mackenzie, I.R.A., Neumann, M., Bigio, E.H., Cairns, N.J., Alafuzoff, I., Kril, J., Kovacs, G.G., Ghetti, B., Halliday, G., Holm, I.E., Ince, P.G., Kamphorst, W., Revesz, T., Rozemuller, A.J.M., Kumar-Singh, S., Akiyama, H., Baborie, A., Spina, S., Dickson, D.W., Trojanowski, J.Q., Mann, D.M.A., 2010. Nomenclature and nosology for neuropathologic subtypes of frontotemporal lobar degeneration: An update. Acta Neuropathol. 119 (1), 1–4.

MacQueen, J., 1967. Some methods for classification and analysis of multivariate observations. Computer Chem. 4, 257–272.

Mercken, M., Vandermeeren, M., Lübke, U., Six, J., Boons, J., Van de Voorde, A., Martin, J.J., Gheuens, J., 1992. Monoclonal antibodies with selective specificity for Alzheimer Tau are directed against phosphatase-sensitive epitopes. Acta Neuropathol. 84 (3), 265–272. https://doi.org/10.1007/BF00227819.

Neumann, M., Sampathu, D.M., Kwong, L.K., Truax, A.C., Micsenyi, M.C., Chou, T.T., Bruce, J., Schuck, T., Grossman, M., Clark, C.M., McCluskey, L.F., Miller, B.L., Masliah, E., Mackenzie, I.R., Feldman, H., Feiden, W., Kretzschmar, H.A., Trojanowski, J.Q., Lee, V.-M.-Y., 2006. Ubiquitinated TDP-43 in frontotemporal lobar degeneration and amyotrophic lateral sclerosis. Science 314 (5796), 130–133. https://doi.org/10.1126/science.1134108.

Neumann, M., Kwong, L.K., Lee, E.B., Kremmer, E., Flatley, A., Xu, Y., Forman, M.S., Troost, D., Kretzschmar, H.A., Trojanowski, J.Q., Lee, V.M.Y., 2009. Phosphorylation of S409/410 of TDP-43 is a consistent feature in all sporadic and familial forms of TDP-43 proteinopathies. Acta Neuropathol. 117 (2), 137–149. https://doi.org/10.1007/s00401-008-0477-9.

Nevler, N., Ash, S., Irwin, D.J., Liberman, M., Grossman, M., 2019. Validated automatic speech biomarkers in primary progressive aphasia. Ann. Clin. Transl. Neurol. 6 (1), 4–14. https://doi.org/10.1002/acn3.653.

Olm, C.A., Kandel, B.M., Avants, B.B., Detre, J.A., Gee, J.C., Grossman, M., McMillan, C. T., 2016. Arterial spin labeling perfusion predicts longitudinal decline in semantic variant primary progressive aphasia. J. Neurol. 263 (10), 1927–1938. https://doi.org/10.1007/s00415-016-8221-1.

Panman, J.L., Venkatraghavan, V., van der Ende, E.L., Steketee, R.M.E., Jiskoot, L.C., Poos, J.M., Dopper, E.G.P., Meeter, L.H.H., Donker Kaat, L., Rombouts, S.A.R.B., Vernooij, M.W., Kievit, A.J.A., Premi, E., Cosseddu, M., Bonomi, E., Olives, J., Rohrer, J.D., Sánchez-Valle, R., Borroni, B., Bron, E.E., Van Swieten, J.C., Papma, J. M., Klein, S., 2021. Modelling the cascade of biomarker changes in GRN -related frontotemporal dementia. J. Neurol. Neurosurg. Psychiatry 92 (5), 494–501.

Rajkomar, A., Dean, J., Kohane, I., 2019. Machine learning in medicine. N. Engl. J. Med. 380 (14), 1347–1358. https://doi.org/10.1056/nejmra1814259.

Seeley, W.W., Crawford, R., Rascovsky, K., Kramer, J.H., Weiner, M., Miller, B.L., Gorno-Tempini, M.L., 2008. Frontal paralimbic network atrophy in very mild behavioral variant frontotemporal dementia. Arch. Neurol. 65 (2), 249–255. https://doi.org/10.1001/archneurol.2007.38.

Ssali, T., Anazodo, U.C., Narciso, L., Liu, L., Jesso, S., Richardson, L., Günther, M., Konstandin, S., Eickel, K., Prato, F., Finger, E., St. Lawrence, K., 2022. Sensitivity of arterial Spin labeling for characterization of longitudinal perfusion changes in Frontotemporal dementia and related disorders. NeuroImage: Clinical 35, 102853. https://doi.org/10.1016/j.nicl.2021.102853.

Staffaroni, A. M., Ljubenkov, P. A., Kornak, J., Cobigo, Y., Datta, S., Marx, G., Walters, S. M., Chiang, K., Olney, N., Elahi, F. M., Knopman, D. S., Dickerson, B. C., Boeve, B. F., Gorno-Tempini, M. L., Spina, S., Grinberg, L. T., Seeley, W. W., Miller, B. L., Kramer, J. H., … Rosen, H. J. (2019). Longitudinal multimodal imaging and clinical endpoints for frontotemporal dementia clinical trials. *Brain*, *142*(2), 443–459. https://doi.org/10.1093/brain/awy319.

Tan, K.S., Libon, D.J., Rascovsky, K., Grossman, M., Xie, S.X., 2013. Differential longitudinal decline on the mini-mental state examination in frontotemporal lobar degeneration and alzheimer disease. Alzheimer Dis. Assoc. Disord. 27 (4), 310–315. https://doi.org/10.1097/WAD.0b013e31827bdc6f.

Toledo, J.B., Van Deerlin, V.M., Lee, E.B., Suh, E., Baek, Y., Robinson, J.L., Xie, S.X., McBride, J., Wood, E.M., Schuck, T., Irwin, D.J., Gross, R.G., Hurtig, H., McCluskey, L., Elman, L., Karlawish, J., Schellenberg, G., Chen-Plotkin, A., Wolk, D., Grossman, M., Arnold, S.E., Shaw, L.M., Lee, V.-Y., Trojanowski, J.Q., 2014. A platform for discovery: The University of Pennsylvania Integrated Neurodegenerative Disease Biobank. Alzheimer's and Dementia 10 (4), 477.

Tustison, N.J., Avants, B.B., Cook, P.A., Zheng, Y., Egan, A., Yushkevich, P.A., Gee, J.C., 2010. N4ITK: Improved N3 bias correction. IEEE Trans. Med. Imaging 29 (6), 1310–1320. https://doi.org/10.1109/TMI.2010.2046908.

Tustison, N.J., Cook, P.A., Klein, A., Song, G., Das, S.R., Duda, J.T., Kandel, B.M., van Strien, N., Stone, J.R., Gee, J.C., Avants, B.B., 2014. Large-scale evaluation of ANTs and FreeSurfer cortical thickness measurements. Neuroimage 99, 166–179. https://doi.org/10.1016/j.neuroimage.2014.05.044.

Venkatraghavan, V., Bron, E.E., Niessen, W.J., Klein, S., 2019. Disease progression timeline estimation for Alzheimer's disease using discriminative event based modeling. Neuroimage 186 (August 2018), 518–532. https://doi.org/10.1016/j.neuroimage.2018.11.024.

Whitwell, J.L., Jack, C.R., Parisi, J.E., Knopman, D.S., Boeve, B.F., Petersen, R.C., Ferman, T.J., Dickson, D.W., Josephs, K.A., 2007. Rates of cerebral atrophy differ in different degenerative pathologies. Brain 130 (4), 1148–1158. https://doi.org/10.1093/brain/awm021.

Whitwell, J.L., Jack, C.R., Senjem, M.L., Parisi, J.E., Boeve, B.F., Knopman, D.S., Dickson, D.W., Petersen, R.C., Josephs, K.A., 2009a. MRI correlates of protein deposition and disease severity in postmortem frontotemporal lobar degeneration. Neurodegener. Dis. 6 (3), 106–117. https://doi.org/10.1159/000209507.

Whitwell, J.L., Przybelski, S.A., Weigand, S.D., Ivnik, R.J., Vemuri, P., Gunter, J.L., Senjem, M.L., Shiung, M.M., Boeve, B.F., Knopman, D.S., Parisi, J.E., Dickson, D.W., Petersen, R.C., Jack, C.R., Josephs, K.A., 2009b. Distinct anatomical subtypes of the behavioural variant of frontotemporal dementia: A cluster analysis study. Brain 132 (11), 2932–2946. https://doi.org/10.1093/brain/awp232.

Whitwell, J.L., Jack, C.R., Parisi, J.E., Knopman, D.S., Boeve, B.F., Petersen, R.C., Dickson, D.W., Josephs, K.A., 2011. Imaging signatures of molecular pathology in behavioral variant frontotemporal dementia. J. Mol. Neurosci. 45 (3), 372–378. https://doi.org/10.1007/s12031-011-9533-3.

Whitwell, J.L., Weigand, S.D., Boeve, B.F., Senjem, M.L., Gunter, J.L., Dejesus-Hernandez, M., Rutherford, N.J., Baker, M., Knopman, D.S., Wszolek, Z.K., Parisi, J. E., Dickson, D.W., Petersen, R.C., Rademakers, R., Jack, C.R., Josephs, K.A., 2012. Neuroimaging signatures of frontotemporal dementia genetics: C9ORF72, tau, progranulin and sporadics. Brain 135 (3), 794–806. https://doi.org/10.1093/brain/aws001.

Wilson, S.M., Ogar, J.M., Laluz, V., Growdon, M., Jang, J., Glenn, S., Miller, B.L., Weiner, M.W., Gorno-Tempini, M.L., 2009. Automated MRI-based classification of primary progressive aphasia variants. Neuroimage 47 (4), 1558–1567. https://doi.org/10.1016/j.neuroimage.2009.05.085.

Wood, E.M., Falcone, D., Suh, E., Irwin, D.J., Alice, S., Lee, E.B., Xie, S.X., Van Deerlin, V. M., Chen-Plotkin, A.S., Lee, E.B., Xie, S.X., Van Deerlin, V.M., Grossman, M., Alice, S., Lee, E.B., Xie, S.X., Van Deerlin, V.M., 2013. Development and validation of pedigree classification criteria for frontotemporal lobar degeneration. J. Am. Med. Assoc.: Neurology 70 (11), 1411–1417. https://doi.org/10.1001/jamaneurol.2013.3956.

Young, A.L., Oxtoby, N.P., Daga, P., Cash, D.M., Fox, N.C., Ourselin, S., Schott, J.M., Alexander, D.C., 2014. A data-driven model of biomarker changes in sporadic Alzheimer's disease. Brain 137 (9), 2564–2577. https://doi.org/10.1093/brain/awu176.

Young, A.L., Marinescu, R.V., Oxtoby, N.P., Bocchetta, M., Yong, K., Firth, N.C., Cash, D. M., Thomas, D.L., Dick, K.M., Cardoso, J., van Swieten, J., Borroni, B., Galimberti, D., Masellis, M., Tartaglia, M.C., Rowe, J.B., Graff, C., Tagliavini, F., Frisoni, G.B., Laforce, R., Finger, E., de Mendonça, A., Sorbi, S., Warren, J.D., Crutch, S., Fox, N.C., Ourselin, S., Schott, J.M., Rohrer, J.D., Alexander, D.C., 2018. Uncovering the heterogeneity and temporal complexity of neurodegenerative diseases with Subtype and Stage Inference. Nat. Commun. 9 (1) https://doi.org/10.1038/s41467-018-05892-0.

Zuendorf, G., Kerrouche, N., Herholz, K., Baron, J.-C., 2003. Efficient principal component analysis for multivariate 3D voxel-based mapping of brain functional imaging data sets as applied to FDG-PET and normal aging. Hum. Brain Mapp. 18 (1), 13–21. https://doi.org/10.1002/hbm.10069.